J. Plasma Physics (2008), *vol.* 74, *part* 1, *pp.* 53–64. © 2007 Cambridge University Press
doi:10.1017/S0022377807006538 First published online 22 May 2007 Printed in the United Kingdom

Parallel electric fields: variations in space and time on auroral field lines

J. VEDIN and K. RÖNNMARK

Department of Physics, Umeå University, SE-90187 Umeå, Sweden
(jorgen.vedin@space.umu.se)

(Received 16 January 2007, revised 23 January 2007, accepted 12 February 2007)

Abstract. We present results from a particle–fluid simulation of auroral electrons and discuss the distribution of parallel electric fields along auroral field lines and the processes occurring during the build up of these electric fields. Neglecting field-aligned ion dynamics, the main potential drop has a width of about 5000 km and is centered at an altitude of roughly 5000 km. We find that the gradient in the potential becomes steeper and the build up of the potential drop becomes faster if the temperature of the magnetospheric electrons is lower.

1. Introduction

Static parallel electric fields on auroral field lines have been addressed in numerous theoretical studies (e.g., Persson 1966; Knight 1973; Whipple 1977; Chiu and Schulz 1978; Stern 1981; Jasperse and Grossbard 2000). In particular, Knight (1973) has shown that the electrostatic potential drop between the equatorial plane and the ionosphere for typical auroral currents is of the order of kilovolts. The time-evolution of the parallel electric fields can be described by fluid models (e.g., Goertz and Boswell 1979; Lysak and Dum 1983; Streltsov et al. 1998; Rönnmark and Hamrin 2000; Streltsov and Lotko 2003), but none of these dynamic models describe how to generate a state consistent with the current–voltage relation presented in Knight (1973). The missing ingredient in the fluid models is a proper description of the electron temperature evolution, which is crucial for the build up of parallel electric fields as shown in Vedin and Rönnmark (2005). The temperature is usually determined from an equation of state, but for the auroral acceleration process with large field-aligned flows in an inhomogeneous magnetic field there is no local equation of state (Ramos 2003; Vedin and Rönnmark 2005). Therefore, fluid models have been unable to describe the auroral electrons in the presence of large field-aligned electric fields.

The particle–fluid model presented in Vedin and Rönnmark (2006) compensates for the drawbacks of a pure fluid model by including effects of detailed particle trajectories. The particles and the electromagnetic fields evolve self-consistently in the presence of a dipolar magnetic field and strong field-aligned density gradients. The model shows that when a current is driven along the field lines, the electron temperature increases and allows a potential drop consistent with Knight's current–voltage relation to be sustained.

In this paper we will discuss parallel electric fields in a quasi-neutral and quasi-stationary plasma with a significant field-aligned current. We will also show how

https://doi.org/10.1017/S0022377807006538 Published online by Cambridge University Press

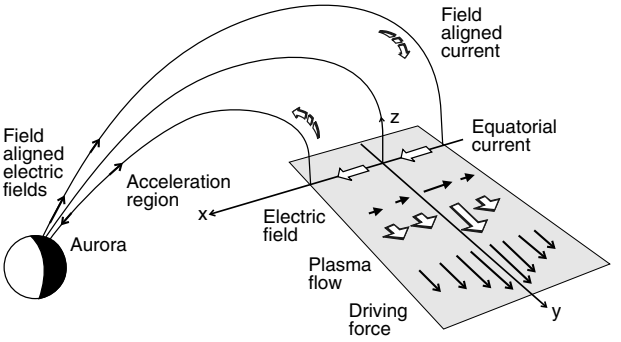


Figure 1. The geometry of the auroral current circuit and the generator region in the equatorial magnetosphere. The curvature of the magnetic field lines is neglected in our model equations.

this electric field is built up when the current increases, with a focus on the upward current region. First, in the next section we give a brief review of the particle–fluid model originally presented in Vedin and Rönnmark (2006). Then, we present the quasi-stationary solution in Sec. 3, and the build-up process in Sec. 4. Finally, we discuss the results and future developments of the model in Sec. 5.

2. Particle–fluid model

The particle–fluid model was originally presented in Vedin and Rönnmark (2006), but the model presentation only contained a few selected results to show that the model was properly working. In this study, we focus on results from the model and in particular we will describe what determines the field-aligned distribution of the parallel electric field that accelerates the auroral electrons. We will also discuss parameters that determine the time scale on which the quasi-static parallel electric fields are built up. Before presenting the results in the following sections, we first briefly introduce the particle–fluid model. The details of the model with the governing equations are given in Vedin and Rönnmark (2006) and a complementary description of the implementation can be found in Vedin and Rönnmark (2007b). In this study we use the same model parameters as in the original model presentation unless otherwise stated in a specific result.

The geometry of the auroral current circuit and the generator region in the equatorial magnetosphere is sketched in Fig. 1. We introduce a coordinate system based on the flux tube geometry, with z along the magnetic field lines, x increasing to the Earth and y to the west. The origin of this coordinate system is at a point where an auroral field line crosses the equatorial plane. We perform the simulations in a two-dimensional plane described by $0 < z < L_z$, $-L_x < x < L_x$, where $L_z = 5.5 \times 10^4$ km (or $8.6 R_{\rm E}$) and L_x is 2000 km at the equatorial plane and 78.6 km in the ionosphere owing to the convergence of the magnetic field lines. When presenting the results we will also use the height $h = L_z - z$ above the ionospheric boundary. We use a dipolar magnetic field $B_z(z)$ with a strength $B_{\rm M} = 0.0864$ μT at $z = 0$ and $B_{\rm I} = 56$ μT at the ionospheric boundary.

The electron distributions in the model are characterized by the density and temperature of the source distributions at the boundaries. At the equatorial boundary, the electrons have a Maxwellian velocity distribution with a loss cone, and a density $n_{\rm M}$ and a temperature $T_{\rm M}$. The electrons at the ionospheric boundary are

https://doi.org/10.1017/S0022377807006538 Published online by Cambridge University Press

also Maxwellian with a loss cone, and the corresponding parameters are $n_{\rm I}$ and $T_{\rm I}$. These electron parameters are used to initialize the electron fluid and to determine the initial number of particles at any point z along the field line. As the simulation runs, particles are continuously injected from the boundaries to compensate for the particles that move outside the simulation domain.

In the model, a prescribed generator force at the equatorial end of the flux tube sets up the dynamics by driving a field-aligned current. The changes in the current are associated with oblique shear Alfvén waves, which contain a field-aligned component of the electric field that can accelerate the electrons. The accelerated electrons mirror in the magnetic field gradient and form a velocity distribution with higher temperatures than prior to the acceleration. The increased temperatures correspond to a pressure gradient that can balance a quasi-static electric field in the acceleration region. As long as the current increases, the pressure gradient and the field-aligned electric field keep increasing. Finally, the generator force relaxes to a stationary value and the fields converge to a quasi-stationary state where the field-aligned potential drop and the generator-driven current density fulfill Knight's current–voltage relation (Knight 1973).

3. Quasi-stationary state

We initialize the simulations without any net current, and in this initial state the potential drop only contains a small ($\lesssim$10 V) ambipolar contribution. The ambipolar potential in our model is described by

$$\phi_{\rm amb}(z) = \begin{cases} 0, & z < z_{\rm amb} \\ \Phi_{\rm amb}\left[\left(\dfrac{z}{z_{\rm amb}}\right)^{\alpha} - 1\right] \Big/ \left[\left(\dfrac{L_z}{z_{\rm amb}}\right)^{\alpha} - 1\right], & z \geqslant z_{\rm amb} \end{cases} \tag{3.1}$$

where $z_{\rm amb}$ and α are adjustable parameters with default values $z_{\rm amb} = 0.9L_z$ and $\alpha = 1$. The value of $z_{\rm amb}$ determines the location of the acceleration region, but it will not otherwise significantly affect the results and neither will the value of α. The value of $\Phi_{\rm amb}$ is determined from the initial condition $j_z = 0$ and therefore depends on the density and temperature of the source distributions in the magnetosphere and ionosphere. If $n_{\rm M}$ or $T_{\rm M}$ are reduced, the current of magnetospheric electrons ($\sim n_{\rm M}\sqrt{T_{\rm M}}$) will decrease. To maintain $j_z = 0$, the current of ionospheric electrons must be reduced, and this is accomplished by a larger $\Phi_{\rm amb}$. A larger $\Phi_{\rm amb}$ will also reduce the initial density of ionospheric electrons as in Fig. 2, while the density of magnetospheric electrons is approximately independent of $\Phi_{\rm amb}$ since $T_{\rm M} \gg \Phi_{\rm amb}$. We assume the initial state to be quasi-neutral and the ion density profile is therefore also affected by the changed $\Phi_{\rm amb}$.

If we increase the current density j_z, the field-aligned potential drop $\Delta\phi$ will increase according to Knight's linear current–voltage relation (Knight 1973)

$$\Delta\phi \approx -\frac{\sqrt{2\pi m T_{\rm M}}}{n_{\rm M} e^2} j_{z\rm I} - \frac{T_{\rm M}}{e} \equiv K j_{z\rm I} - \frac{T_{\rm M}}{e}, \tag{3.2}$$

where $j_{z\rm I} = B_{\rm I}/B_z j_z$ is the current density at the ionosphere, m is the electron mass and $-e$ is the electron charge. To ensure that the solution remains quasi-neutral, the distribution of the potential drop along the field line must be such that it keeps the electron density equal to the ion density, which we assume to be time independent. The shape of the potential will then depend on the ion density profile, the electron

https://doi.org/10.1017/S0022377807006538 Published online by Cambridge University Press

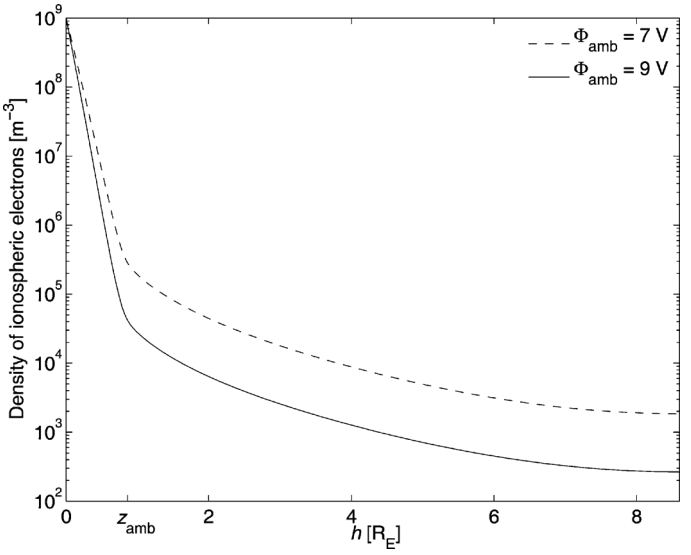


Figure 2. The density of electrons originating from the ionospheric boundary for two different values of Φ_{amb}. The density of magnetospheric electrons is approximately independent of Φ_{amb} and does in this case vary from 3×10^5 m^{-3} at the equatorial plane to 1.5×10^5 m^{-3} at the ionosphere.

parameters n_{M} and T_{M}, and the magnitude of the potential drop. However, both the ion density profile (via Φ_{amb}) and the total potential drop (via (3.2)) depends on n_{M} and T_{M}.

Thus, the values of n_{M} and T_{M} have the greatest impact on the potential profile. Let us start by considering the changes that follow from a reduced T_{M}. A lower T_{M} will in the initial state, as mentioned above, result in a lower density of ionospheric electrons in the acceleration region. When the potential drop increases, the density of magnetospheric electrons in the acceleration region will increase. The density of ionospheric electrons must then be further reduced to maintain quasi-neutrality, but this is harder to achieve in the case of low T_{M} where the density of ionospheric electrons is low already from the start. Furthermore, for a potential satisfying

$$\frac{d^2\phi(z')}{dB(z')^2} \leqslant 0 \quad \text{for all } z' \leqslant z, \tag{3.3}$$

and for a prescribed current, the increase in the magnetospheric electron density at a point in the acceleration region will be stronger for a lower T_{M} (Janhunen 1999). Thus, there are two effects adding to the difficulty of keeping the plasma quasi-neutral when T_{M} is small.

To achieve quasi-neutrality the potential can then be adjusted to have a steeper gradient. This implies that condition (3.3) is not satisfied, and we must use the algorithm presented in Vedin and Rönnmark (2004) to compute the regions in the velocity plane accessible to magnetospheric electrons. The sharper potential gradient reduces the regions of accessibility, thus reducing the magnetospheric electron density. Then, the ionospheric electrons can more easily maintain quasi-neutrality.

Now we will continue by considering the changes in the potential profile that follow from a reduced n_{M}. A lower n_{M} will in the initial state result in a lower density of ionospheric electrons in the acceleration region. However, the reduction

https://doi.org/10.1017/S0022377807006538 Published online by Cambridge University Press

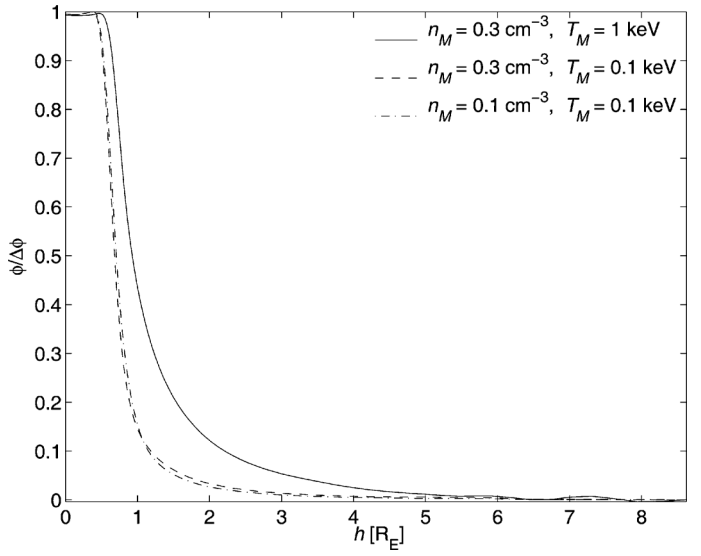


Figure 3. The normalized potential $\phi/\Delta\phi$ as a function of altitude for three different configurations.

of the ionospheric density in the acceleration region is approximately equal to the reduction made in n_{M}. Therefore, the fraction of the total density in the acceleration region consisting of ionospheric electrons is not changed. As the potential drop increases, the density of magnetospheric electrons will increase in the acceleration region, but this increase can now be balanced by a reduction of the ionospheric electron density with a potential profile that is independent of the value of n_{M}. Thus, if n_{M} is reduced, there is no need for a sharper potential gradient to maintain quasi-neutrality. The potential profiles for three different combinations of T_{M} and n_{M} are shown in Fig. 3 when the current density is about 1 μA m^{-2}. This confirms that the value of T_{M} is important for the potential profile, and that a lower temperature leads to a sharper gradient.

There are two comments about the above discussion. First, note that Φ_{amb} depends not only on n_{M} and T_{M}, but also on the corresponding values n_{I} or T_{I} of the ionospheric electrons. A change in n_{I} will, like a change in n_{M}, not affect the shape of the potential distribution, but an increased T_{I} will, like a reduced T_{M}, create a more localized potential drop. Second, the above discussion is valid for a constant current density. If the generator conditions are such that a weaker or stronger current is driven in the flux tube, the potential drop will be affected according to (3.2). Since the potential drop will affect the increase in magnetospheric electron density in the acceleration region, it will also affect the shape of the potential. For a stronger current density, the potential drop increases and the potential drop must then be more localized for the electrons to maintain quasi-neutrality. Thus, an increased current has a similar effect on the quasi-stationary potential distribution as a reduced temperature T_{M}.

4. Build up of parallel electric fields

Using the particle–fluid model we can describe the build up of parallel electric fields and auroral currents from the initial state to the quasi-stationary state with

https://doi.org/10.1017/S0022377807006538 Published online by Cambridge University Press

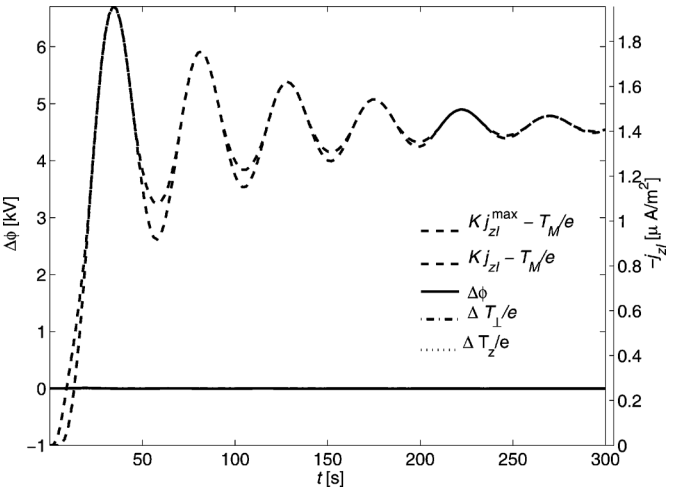


Figure 4. Time evolution of the potential drop together with the current density and the temperature perturbations scaled to kilovolts for the case of isothermal electrons. The fields are extracted from the simulation data at the x-value having the strongest upward current density. The lower value of current density is computed in the acceleration region ($h \approx 5000$ km), while the higher value is the maximum value along the chosen field line. To obtain rescaled current densities comparable to the potential drop we use (3.2). The potential drop and, of course, the temperature perturbations are zero in this isothermal result.

a significant current. In this section we will present results that show the build-up process in the upward current region. To obtain a simple representation of the fields, we have chosen to plot the potential drop as a function of time and to include the temperature perturbations and the current density in the same figure. The current density is converted to a potential drop by using Knight's current–voltage relation (3.2).

We will start by presenting results for isothermal electrons to give a simplified starting point for the physics involved in the build up of auroral currents. Then, we will present the build up for two different values of $T_{\rm M}$, since this is a parameter with great impact on the potential distribution according to the discussion in the previous section.

4.1. Isothermal electrons

By ignoring the particle part of our simulation, we can model isothermal auroral electrons. Note that although the temperature is not varying in time, it is still varying in space owing to the mixing of ionospheric electrons with a source temperature of $T_{\rm I} = 1$ eV and magnetospheric electrons with a source temperature of $T_{\rm M} = 1$ keV. This case is non-physical since the electron temperature is not correctly modeled, and we present the results with the sole purpose of giving a simple introduction to the build-up process. Isothermal electrons can carry strong field-aligned currents without any significant potential drop, and the absence of an acceleration region simplifies the interference pattern of downward and upward propagating Alfvén waves.

Figure 4 shows the build-up process, where the current can be seen as a monotonically increasing component plus an oscillating component due to the interference pattern of Alfvén waves. The period time of these oscillations would in a uniform

https://doi.org/10.1017/S0022377807006538 Published online by Cambridge University Press

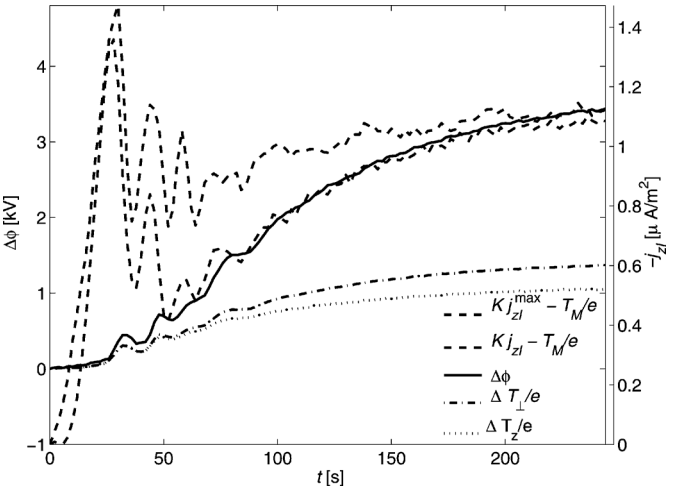


Figure 5. The same type of data as Fig. 4, but from the particle–fluid simulation with $T_{\rm M} = 1$ keV and $n_{\rm M} = 3 \times 10^5$ m^{-3}. The values of the temperature perturbations are the maximum values along the selected field line.

plasma be four times the Alfvén wave transit time $\tau_{\rm A}$ since we are using a generator that acts like a current generator (e.g., Paschmann et al. 2002). A current generator corresponds to the fundamental oscillation of the field line, i.e. Alfvén waves that have a wavelength $\lambda = 4L_z$. Owing to the spatially varying density and magnetic field that results in strong field-aligned gradients in the Alfvén speed, the period time in our configuration is almost eight times $\tau_{\rm A}$. The period time is time independent since the wave reflections only occur at time-independent boundaries such as the ionosphere, the generator, and the gradients in the Alfvén speed. However, the oscillations are slowly damped by the dissipation caused by the finite ionospheric conductivity.

4.2. High $T_{\rm M}$

Figure 5 shows the build-up process for $T_{\rm M} = 1$ keV and $n_{\rm M} = 3 \times 10^5$ m^{-3}. The figure reveals that the potential drop and the current density converge to a state where Knight's current–voltage relation (3.2) holds. The potential drop grows to more than 3 kV, while the temperatures T_z and $T_\perp$ in the acceleration region increase by more than 1 keV. The interference pattern of Alfvén waves is now much more complicated than in the isothermal case. The oscillation period is shorter since waves are now reflected already at the acceleration region, and the period is also time dependent since the acceleration region changes as the parallel electric field increases with time. The oscillations are also more strongly damped in this case. As the potential drop increases, more energy is dissipated as kinetic energy of precipitating electrons.

Figure 5 shows that Knight's current–voltage relation holds already after about 50 s, although the simulation is far from a stationary state at this time. Note that the current–voltage relation is valid for the current at the ionosphere and that there is a difference between the currents $j_{z\rm I}^{\rm max}$ (typically near the generator) and $j_{z\rm I}$ (at the acceleration region) during the build-up phase. This difference indicates that parts of the field-aligned current are closed by perpendicular ion polarization

https://doi.org/10.1017/S0022377807006538 Published online by Cambridge University Press

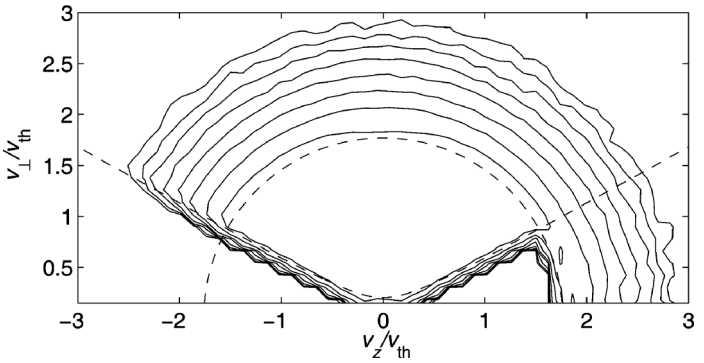


Figure 6. Velocity distribution at an altitude of 4000 km where the potential drop is about 3.0 kV above and 0.2 kV below this altitude. The dashed lines are the loss cone and the turning point boundaries from Chiu and Schulz (1978). The value of the distribution function changes by a factor of two between each consecutive contour. To normalize the velocities we have used the thermal velocity $v_{\rm th} = \sqrt{2T_{\rm M}/m}$.

currents above the acceleration region, but as the simulations converge to a quasi-stationary state this difference goes to zero as expected since $j_{z\rm I}^{\rm max}$ and $j_{z\rm I}$ should be equal in a stationary flux tube.

From Fig. 5 we can also see that the initial increase in the potential drop lags the increase in the current, which can be understood from the initial conditions. If we initialize the simulation without any net field-aligned current, the upward current carried by downgoing magnetospheric electrons is balanced by a downward current carried by upgoing ionospheric electrons. The potential drop needs only increase a few volts to choke the upward flow of ionospheric electrons so that the current increases from zero to the initial current carried by magnetospheric electrons. This small increase in the potential drop will not only stop the current of ionospheric electrons, but it will actually reverse it, causing an upward current as the ionospheric electrons rush down the field line towards the ionosphere. This causes the sudden increase in the current that can be seen in the first 25 s of Fig. 5. When there are no ionospheric electrons left, the current must be maintained by the magnetospheric electrons, and then a significant increase of the potential drop is required.

If we instead initialize the simulation with a net upward current, such that the initial current carried by ionospheric electrons is negligible, the lag in the potential growth will disappear. The current at the acceleration region and the potential drop will then have similar growth rates, and satisfy Knight's current–voltage relation already from the start of the simulation.

Figure 6 shows the velocity distribution of the magnetospheric electrons at an altitude of roughly 4000 km. The potential drop is about 3.0 kV above and 0.2 kV below this altitude. Initially, the velocity distribution is a Maxwellian with a loss cone, and Fig. 6 shows the distribution when the simulation has converged to a quasi-stationary state with a significant current. There are strongly accelerated electrons in the downgoing loss cone and mirroring particles outside the loss cones and the circular turning point boundary. In the forbidden region inside the turning point boundary but outside the loss cones, the phase-space density is high and essentially constant. The particles in this forbidden region are trapped between

https://doi.org/10.1017/S0022377807006538 Published online by Cambridge University Press

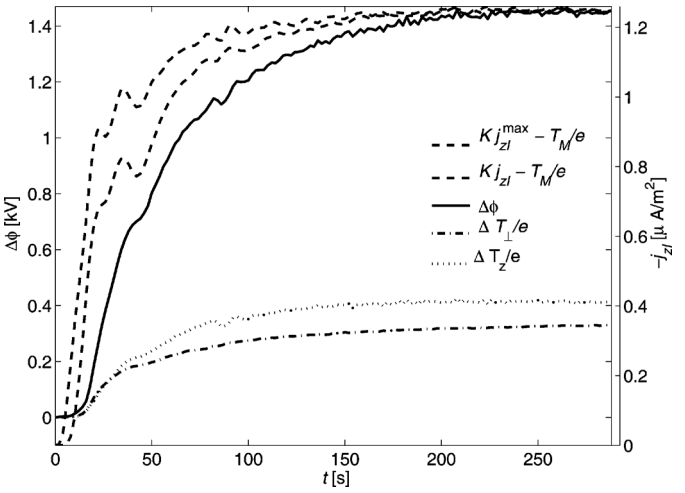


Figure 7. The same type of data as Fig. 5, but with $T_{\rm M} = 0.1$ keV and $n_{\rm M} = 3 \times 10^5$ m^{-3}.

the mirror point and the increasing potential drop. Trapped particles are self-consistently included in the particle–fluid model. The velocity distribution in Fig. 6 has several similarities to those observed on satellites, see, for example, measurements from S3-3 (Croley et al. 1978; Mozer et al. 1980; Omidi et al. 1984), DE-1 (Gurgiolo and Burch 1988), Viking (Louarn et al. 1990), and FAST (Delory et al. 1998; Strangeway et al. 2001).

Comparing the distribution function in Fig. 6 to a Maxwellian with a loss cone we can easily appreciate the need for a correct description of the temperature evolution, since both T_z and $T_\perp$ have increased significantly with time. If this temperature increase is not correctly modeled we cannot expect the simulation to produce large potential drops. We emphasize that the temperature increase is not caused by any local wave heating mechanism, but is a fundamental consequence of the electron acceleration and mirroring in a converging magnetic field.

4.3. Low $T_{\rm M}$

Figure 7 shows the build-up process for $T_{\rm M} = 0.1$ keV and $n_{\rm M} = 3 \times 10^5$ m^{-3}. Compared to the case with a higher $T_{\rm M}$ we see that the potential drop grows much faster in this case and therefore the dissipation due to precipitating electrons damps the Alfvén wave oscillations even faster. A lower $T_{\rm M}$ implies a sharper field-aligned gradient in the potential according to the discussion in Sec. 3. If the gradient in the potential is sharp, there will not be any large electric fields at higher altitudes, and therefore no large ion polarization currents $\sim d_t E_x$. The low-altitude field-aligned current will then increase faster since less of the high-altitude field-aligned current is closed by perpendicular polarization currents above the acceleration region, cf. Figs 5 and 7. A faster growth of the low-altitude current implies a faster growth of the total field-aligned potential drop according to (3.2). Thus, a lower $T_{\rm M}$ implies a sharper gradient in the potential, weaker polarization currents and a faster increase in the low-altitude current and potential drop. As a difference to Fig. 5, where the Knight relation holds during the later part of the build up, the results in Fig. 7 show that the Knight relation only holds in the quasi-stationary state. We cannot fully explain why the Knight relation holds during the build up of the low-altitude

https://doi.org/10.1017/S0022377807006538 Published online by Cambridge University Press

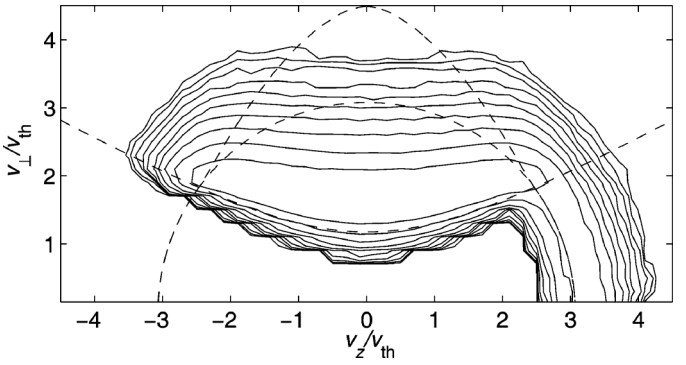


Figure 8. Velocity distribution at an altitude of 4000 km where the potential drop is about 1.0 kV above and 0.4 kV below this altitude. The dashed lines are the loss cone and the turning point boundaries from Chiu and Schulz (1978) and the turning point boundary from the algorithm in Vedin and Rönnmark (2004). The value of the distribution function changes by a factor of two between each consecutive contour.

current and the potential drop if the build up is slow, while it does not hold if the build up is fast.

In Fig. 7 the increase in the parallel temperature is greater than the increase in the perpendicular temperature, while the changes at a higher T_M are the opposite. This can also be seen in the velocity distribution at the acceleration region, which is presented in Fig. 8. For this result, the potential drop is so localized that the turning point boundary must be generalized according to the algorithm in Vedin and Rönnmark (2004). The distorted turning point boundary implies a saddle in the velocity contours at pitch angles close to 90° according to the discussion of velocity distributions presented in Vedin and Rönnmark (2007a) and this leads to a reduced perpendicular temperature.

5. Discussion and conclusions

We have focused on the upward current region, since the present version of the particle–fluid model neglects ion dynamics and high-frequency waves ($\gtrsim$50 Hz) and therefore does not properly describe the downward current region. In particular, the simulations do not produce any significant parallel electric fields in the return current region although observations indicate their presence (Klumpar and Heikkila 1982; Burch et al. 1983; Marklund and Karlsson 2001; Johansson et al. 2004). A time-independent ion density is a reasonable approximation on shorter time scales. However, the build up of a quasi-stationary state can in our model last for a few minutes, which implies that the ions have time to react to the fields. Therefore, an extension of the model to include ion dynamics is important not only for the downward current region but most likely also for the shape of the potential in the upward current region. The neglect of ion dynamics together with simplifications of the ionospheric model also imply that we do not describe the dynamics of visible auroras, such as, for example, vortex structures in black aurora (Shukla et al. 1995).

To include the ion dynamics we need to resolve the ion gyro frequency, which is almost ∼1 kHz at the lowest altitudes. In the present version of the model we

https://doi.org/10.1017/S0022377807006538 Published online by Cambridge University Press

only resolve frequencies below ∼ 50 Hz, which is enough to describe the slow build up associated with Alfvén waves. Although Alfvén waves and quasi-static electric fields are believed to cause the acceleration of the primary auroral electrons, the suppression of higher frequencies implies that we neglect some waves that can be associated with electron and ion acceleration on auroral field lines. These waves include, for example, circularly polarized electromagnetic waves (Shukla et al. 1996), electrostatic ion-cyclotron waves (Shukla and Stenflo 1998), and lower-hybrid waves (Bingham et al. 1984, 2001). For a review on acceleration mechanisms on auroral field lines the reader is referred to Borovsky (1993).

We have in this paper shown how the parallel electric field is built up on auroral field lines. A weak parallel electric field carried by an oblique shear Alfvén wave is a prerequisite for the increase in the electron pressure, and the gradients in the electron pressure are necessary for the build up of a stronger quasi-static parallel electric field. Hence, these two forces are built up balancing each other. Furthermore, we have identified parameters that affect the build-up process and found that the temperature of the magnetospheric electrons is a crucial parameter. Cold magnetospheric electrons will cause a sharper gradient in the field-aligned potential, and this implies a faster build up of the parallel electric field.

Acknowledgements

This research was conducted using the resources of High Performance Computing Center North (HPC2N), and was supported by the Swedish National Graduate School of Space Technology.

References

Bingham, R., Bryant, D. A. and Hall, D. S. 1984 A wave model for the aurora. *Geophys. Res. Lett.* **11**, 327.

Bingham, R., Cairns, R. A., Dendy, R. O., Shapiro, V. D., Shukla, P. K. and Stenflo, L. 2001 Auroral particle acceleration by waves. *Phys. Chem. Earth* **26**, 133.

Borovsky, J. E. 1993 Auroral arc thickness as predicted by various theories. *J. Geophys. Res.* **98**, 6101.

Burch, J. L., Reiff, P. H. and Sugiura, M. 1983 Upward electron beams measured by DE-1: a primary source of dayside region-1 Birkeland currents. *Geophys. Res. Lett.* **10**, 753.

Chiu, Y. T. and Schulz, M. 1978 Self-consistent particle and parallel electrostatic field distribution in the magnetospheric-ionospheric auroral region. *J. Geophys. Res.* **83**, 629.

Croley, D. R., Jr., Mizera, P. F. and Fennell, J. F. 1978 Signature of a parallel electric field in ion and electron distributions in velocity space. *J. Geophys. Res.* **83**, 2701.

Delory, G. T., Ergun, R. E., Carlson, C. W., Muschietti, L., Chaston, C. C., Peria, W., McFadden, J. P. and Strangeway, R. 1998 FAST observations of electron distributions within AKR source regions. *Geophys. Res. Lett.* **25**, 2069.

Goertz, C. K. and Boswell, R. W. 1979 Magnetosphere-ionosphere coupling. *J. Geophys. Res.* **84**, 7239.

Gurgiolo, C. and Burch, J. L. 1988 Simulation of electron distributions within auroral electron regions. *J. Geophys. Res.* **93**, 3989.

Janhunen, P. 1999 On the current–voltage relationship in fluid theory. *Ann. Geophys.* **17**, 11.

Jasperse, J. R. and Grossbard, N. J. 2000 The Alfvén–Fälthammar formula for the parallel E-field and its analogue in downward auroral-aurrent regions. *IEEE Trans. Plasma Sci.* **28**, 1874.

Johansson, T., Figueiredo, S., Karlsson, T., Marklund, G., Fazakerley, A., Buchert, S., Lindqvist, P.-A. and Nilsson, H. 2004 Intense high-altitude auroral electric fields—temporal and spatial characteristics. *Ann. Geophys.* **22**, 2485.

https://doi.org/10.1017/S0022377807006538 Published online by Cambridge University Press

Klumpar, D. M. and Heikkila, W. J. 1982 Electrons in the ionosphere source cone: evidence for runaway electrons as carriers of downward Birkeland currents. *Geophys. Res. Lett.* **9**, 873.

Knight, S. 1973 Parallel electric fields. *Planet. Space Sci.* **21**, 741.

Louarn, P., Roux, A., de Féraudy, H., Le Quéau, D., André, M. and Matson, L. 1990 Trapped electrons as a free energy source for the auroral kilometric radiation. *J. Geophys. Res.* **95**, 5983.

Lysak, R. L. and Dum, C. 1983 Dynamics of magnetosphere-ionosphere coupling including turbulent transport. *J. Geophys. Res.* **88**, 365.

Marklund, G. T. and Karlsson, T. 2001 Characteristics of the auroral particle acceleration in the upward and downward current regions. *Phys. Chem. Earth* **26**, 81.

Mozer, F. S., Cattell, C. A., Hudson, M. K., Lysak, R. L., Temerin, M. and Torbert, R. B. 1980 Satellite measurements and theories of low altitude auroral particle acceleration. *Space Sci. Rev.* **27**, 155.

Omidi, N., Wu, C. S. and Gurnett, D. A. 1984 Generation of auroral kilometric and Z mode radiation by the cyclotron maser mechanism. *J. Geophys. Res.* **89**, 883.

Paschmann, G., Haaland, S. and Treumann, R. 2002 Auroral plasma physics. *Space Sci. Rev.* **103**, 322.

Persson, H. 1966 Electric field parallel to the magnetic field in a low-density plasma. *Phys. Fluids* **9**, 1090.

Ramos, J. J. 2003 Dynamic evolution of the heat fluxes in a collisionless magnetized plasma. *Phys. Plasmas* **10**, 3601.

Rönnmark, K. and Hamrin, M. 2000 Auroral electron acceleration by Alfvén waves and electrostatic fields. *J. Geophys. Res.* **105**, 25333.

Shukla, P. K., Birk, G. T. and Bingham, R. 1995 Vortex streets driven by sheared flow and applications to black aurora. *Geophys. Res. Lett.* **22**, 671.

Shukla, P. K., Stenflo, L., Bingham, R. and Dendy, R. O. 1996 Pondermotive force acceleration of ions in the auroral region. *J. Geophys. Res.* **101**, 27449.

Shukla, P. K. and Stenflo, L. 1998 Interpretations of new features of time domain electric-field structures in the auroral acceleration region. *Ann. Geophys.* **16**, 889.

Stern, D. P. 1981 One-dimensional models of quasi-neutral parallel electric fields. *J. Geophys. Res.* **86**, 5839.

Strangeway, R. J., Ergun, R. E., Carlson, C. W., McFadden, J. P., Delory, G. T. and Pritchett, P. L. 2001 Accelerated electrons as the source of auroral kilometric radiation. *Phys. Chem. Earth* **26**, 145.

Streltsov, A. V. and Lotko, W. 2003 Reflection and absorption of Alfvénic power in the low-altitude magnetosphere. *J. Geophys. Res.* **108**, 8016.

Streltsov, A. V., Lotko, W., Johnson, J. R. and Cheng, C. Z. 1998 Small-scale, dispersive field line resonances in the hot magnetospheric plasma. *J. Geophys. Res.* **103**, 26559.

Vedin, J. and Rönnmark, K. 2004 A linear auroral current–voltage relation in fluid theory. *Ann. Geophys.* **22**, 1719.

Vedin, J. and Rönnmark, K. 2005 Electron pressure effects on driven auroral Alfvén waves. *J. Geophys. Res.* **110**, A01214.

Vedin, J. and Rönnmark, K. 2006 Particle-fluid simulation of the auroral current circuit. *J. Geophys. Res.* **111**, A12201.

Vedin, J. and Rönnmark, K. 2007a Estimating auroral double layer properties from electron velocity distributions. *Geophys. Res. Lett.* (submitted).

Vedin, J. and Rönnmark, K. 2007b Implementing a particle–fluid model of auroral electrons. *Lecture notes in Computer Science* (in press).

Whipple, E. C., Jr. 1977 The signature of parallel electric fields in a collisionless plasma. *J. Geophys. Res.* **82**, 1525.

https://doi.org/10.1017/S0022377807006538 Published online by Cambridge University Press